Sixth International Conference on Durability of Concrete Structures
18 - 20 July 2018
University of Leeds, Leeds, West Yorkshire, LS2 9JT, United Kingdom

Paper Number MID05

# Improving the spacer-concrete interface for bond strength and durability

F. Muslim, H.S. Wong and N.R. Buenfeld
Concrete Durability Group, Department of Civil and Environmental Engineering, Imperial College London, UK

## ABSTRACT

*Spacers are important devices in reinforced concrete that are used to support reinforcing steel during concreting in order to achieve the required concrete cover. They are placed at every meter length or less of steel reinforcement and left permanently in the structure. However, it has been shown that the interface between spacer and concrete is highly porous and microcracked. This lowers the resistance of the concrete cover to the ingress of aggressive agents causing degradation. This study aims to address this problem by improving spacer design to enhance bond strength and durability of the spacer-concrete interface. Cementitious spacers with a range of surface textures were produced prior to casting into concrete. Samples were prepared with CEM I Portland cement at a water/cement (w/c) ratio of 0.4 and cured for 1, 7, and 28 days in a fog room and then conditioned at 50°C to equilibrium moisture content. The spacer-concrete interface was then tested for tensile bond strength and mass transport properties including oxygen diffusivity, oxygen permeability, and water absorption. The measured surface properties were correlated to the measured bond strength and transport properties to establish the effects of surface texture on the spacer-concrete interface.*

**Keywords:** Reinforcement spacer, spacer-concrete interface, surface texture, interface bond strength, transport properties, durability.

## 1.0 INTRODUCTION

The function of a spacer in reinforced concrete is to support and secure reinforcing steel in proper position during construction so that the required concrete cover is achieved (BS 7973-1:2001). Following codes of practice and design standards for concrete structures, a single spacer should be placed at every meter length or less of reinforcement. As such, the spacer plays a vital role in the structure, and a typical concrete structure contains thousands of spacers in the cover zone (BS 7973-2:2001). A good quality concrete cover with the correct thickness is essential to ensure the durability of the whole structure, in particular, to protect reinforcing steel against corrosion. However, Alzyoud *et al.* (2016) found that the interface between spacer and surrounding concrete is highly porous and microcracked. This is due to poor particle packing at the interface, drying-induced shrinkage and low bond strength between spacer and concrete. The porous interface facilitates penetration of aggressive species such as chloride ions that could accelerate the initiation of reinforcement corrosion (See Fig. 1).

A number of studies have been carried out on the interface bond strength in the field of concrete repairs. Pigeon and Saucier (1992) reported that the interface between concrete substrate and repair materials is very similar to the bond between aggregates and cement paste. It is generally considered a weak zone. Several mechanisms contribute to bond strength, amongst these, mechanical interlocking is considered the dominant mechanism compared to adhesion and chemical bonding between two materials. As such, various attempts were conducted to improve mechanical interlocking between substrate and repair material. Julio *et al.* (2004) and Garbacz *et al.* (2005) showed that surface roughness had a significant influence and found that sand-blasting was an effective surface treatment method. Other methods including grinding, jack-hammering, wire brushing, milling, and hydro-jetting or shot-blasting were also tested. However, such treatments generated more cracks and caused deterioration of the near-surface layer.

The aim of this study is to investigate the influence of surface texture on the bond strength and durability of the spacer-concrete interface. Cementitious spacers of different surface textures were prepared, cast in concrete, and then tested for splitting tensile strength. Moreover, the study also examined the influence of the surface texture on mass transport properties including oxygen diffusivity, oxygen permeability, and water sorptivity. Finally, the measured surface properties were correlated to the measured bond strength and transport properties to establish the effects of surface texture on the spacer-concrete interface.

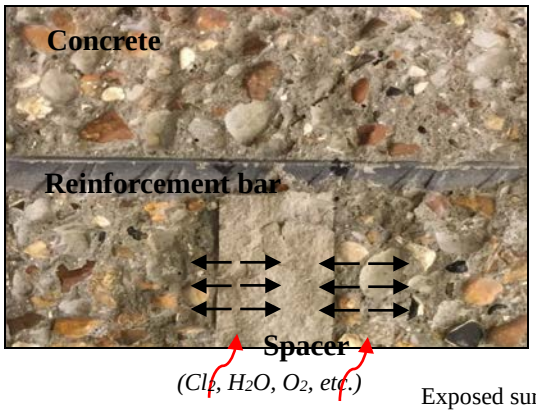


**Fig. 1.** Example of cross-section of reinforced concrete showing the placement of steel reinforcement on a cementitious spacer to achieve a designed cover. Aggressive species (i.e. chloride, water, and oxygen) may penetrate through the porous interface between spacer and concrete. Black arrows indicate the possibility of debonding due to, for example, shrinkage-induced cracks in concrete or thermal effects

## 2.0 EXPERIMENTAL DETAILS

### 2.1 Materials and mixture proportion

Cementitious spacer and concrete were prepared with the same mix; Portland cement with specific gravity of 3.15, water-cement ratio (w/c) of 0.4, total aggregate content of 70%, and sand to total aggregate content ratio of 0.4. The mix achieved a 28-day compressive strength of 66.6 MPa, which conforms to the requirements of BS 7973-1:2001. The Portland cement used complies with BS EN 197-1:2011 CEM I. The aggregates were Thames Valley gravel (<10 mm) and sand (<5 mm) complying with BS 882 medium grading. The mix proportions calculated using the absolute volume method are shown in Table 1.

**Table 1**. Mix proportions of spacer and concrete

| W/C ratio | CEM I (kg/m$^3$) | Water (kg/m$^3$) | Sand (kg/m$^3$) | Gravel (kg/m$^3$) |
|---|---|---|---|---|
| 0.4 | 418 | 167 | 728 | 1092 |

### 2.2 Sample preparation

Cylindrical samples were prepared in steel moulds of 100 mm diameter and 50 mm height. Each sample contained half-spacer and half-concrete for bond strength and mass transport testing.

In order to cast the half spacer, a wooden block with silicon attachment was inserted into the steel ring as shown in Fig. 1. The surface texture of the spacer was varied by varying the texture of the silicone attachment. A range of silicone attachments with different surface textures were used. The shape, maximum profile depth and total surface area of each texture are shown in Table 2. The maximum profile depth is defined as the distance between highest and lowest point of the profile. A wooden plate was then tightly screwed on to the top of the mould assembly so that the wooden blocks did not move during compaction. The spacers were cast, cured and then re-inserted back into the corresponding steel ring moulds as shown in Fig. 3a. The wooden plate was then fixed on to the top of the spacers and fresh concrete was cast against the prefabricated spacers as shown in Fig. 3b.

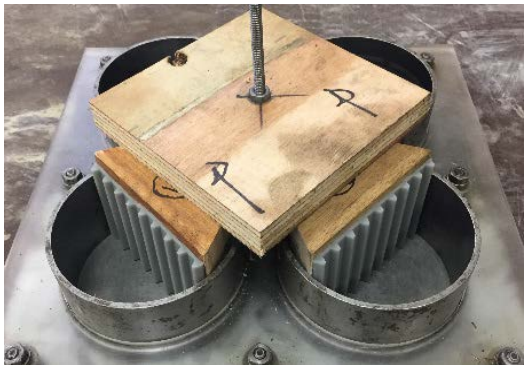

**Fig. 2.** Set-up for preparing spacers with modified surface texture

**Table 2.** Shape, profile and area of various surface textures

| Name | Shape | Max. profile depth (mm) | Surface area (mm$^2$) |
|---|---|---|---|
| Control – flat (CO) | | - | 5000 |
| Grooves-horizontal (GH) | | 4 | 6025 |
| Grooves-vertical (GV) | | 4 | 6025 |
| Half-sphere (HS) | | 8 | 9870 |
| Pyramid (PY) | | 9 | 8028 |

### 2.3 Mixing, curing and conditioning

The procedures for mixing, curing and conditioning the spacer and concrete are the same and are summarised here. Cement and aggregates were firstly dry mixed for 30 s in a 30-litre capacity pan mixer. Water was then added and wet mixing was carried out for a further 3 min.

A vibrating table with adjustable intensity was used for compaction. Samples were compacted in two equal-depth layers until no significant amount of air bubbles escaped the surface. During compaction of the spacers, the fresh mix flows over the silicone mould and fills the crevices to produce the desired texture. Subsequently, fresh concrete is cast against the prefabricated spacer (Fig. 2b) to produce a sample with spacer-concrete interface for testing.

The samples were then covered with plastic sheet and wet hessian at room temperature for the first 24 h, then demoulded and cured in a fog room (100% RH) at 20°C for 1, 7 and 28 days prior to tensile strength testing. Replicate samples were prepared and cured for 7d, then conditioned at 50°C, 10±2% RH to constant mass prior to transport testing.

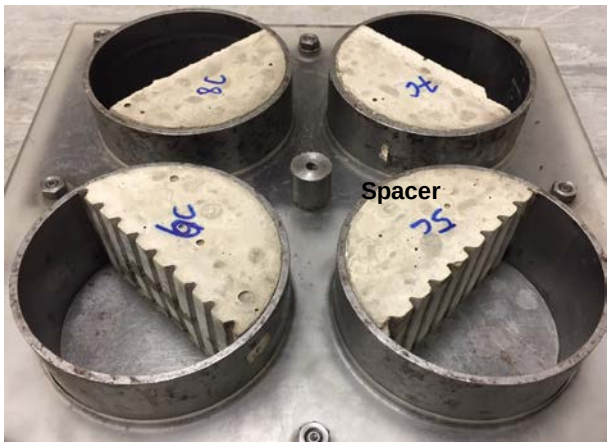


a) Half-spacers in steel mould assembly

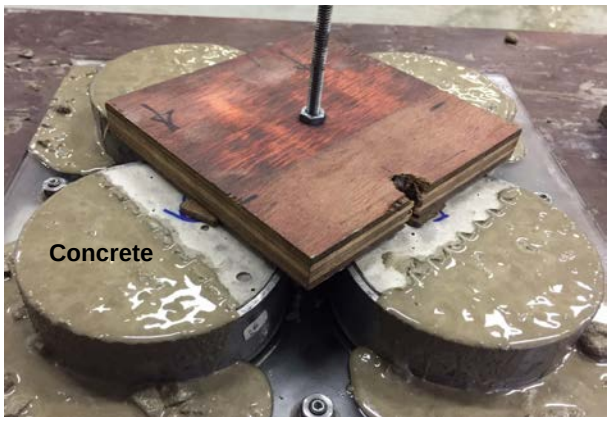


b) Casting concrete against prefabricated spacers

**Fig. 3.** Set-up for preparing 100Ø mm disc samples containing half-spacer and half-concrete

### 2.4 Splitting tensile strength test

Splitting tensile testing, using the Brazilian test conforming to BS EN 12390-6:2000, was carried out to determine the interface bond strength between spacer and concrete. This is based on applying two opposing compressive point loads perpendicularly to the axis of the cylindrical sample to induce a uniform tensile stress over the interfacial plane (Fig 4). Special care was taken when positioning the sample so that the spacer-concrete interface aligned with the applied load. Three replicates were tested, and the results averaged for each case.

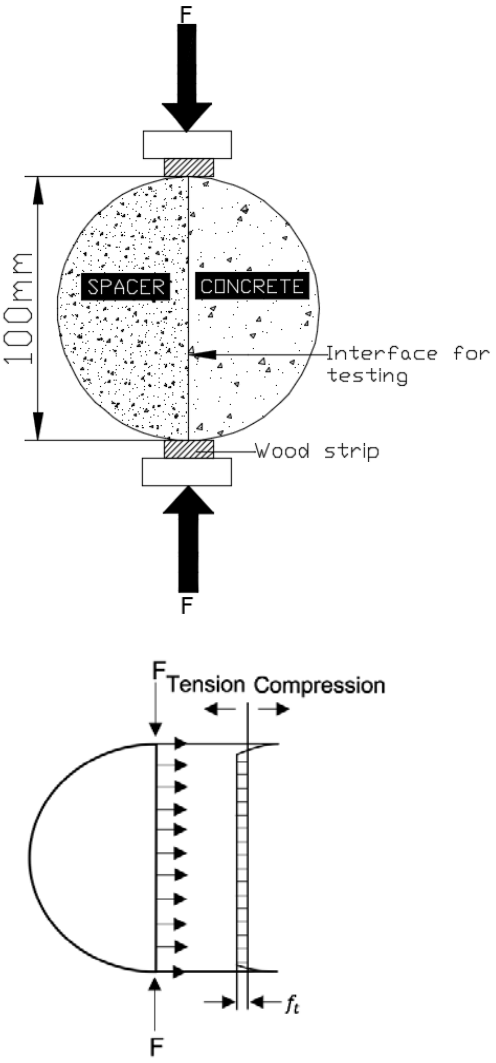


**Fig. 4. (a)** Schematic diagram of splitting tensile strength test for spacer-concrete interface; (b) Stress distribution assumed along the diameter of sample

Assuming a uniform tensile stress across the interfacial plane, the splitting tensile strength $f_t$ can be simplified as:

$$f_t = \frac{2F}{\pi L d} \quad (1)$$

Where $f_t$ is the tensile splitting strength (MPa), $F$ is the maximum applied load (N), $L$ is the length of the

specimen (mm), and *d* is the diameter of specimen (mm).

### 2.5 Mass transport properties

The 7d samples were conditioned at 50°C to constant mass and then tested for oxygen diffusivity, oxygen permeability, and water sorptivity using two replicates for each case. Full details of the tests are given in Wong *et al.* (2007) and are summarised here.

Oxygen diffusivity and oxygen permeability were measured by placing the sample in a test cell and applying a 15 kN compression to the surrounding silicone rubber ring to seal the sample to prevent side leakage (Wu *et al.*, 2014). To determine oxygen diffusivity, opposite faces of the sample were exposed to oxygen and nitrogen gases at the same pressure, which diffused in opposite directions through the sample. A zirconia analyser was used to measure the oxygen concentration in the outflow stream. To determine oxygen permeability, steady-state outflow rates were measured for three input gas pressures of 0.5, 1.5 and 2.5 bars above atmospheric. Permeability at each pressure was calculated by applying Darcy's law for compressible fluids, and the intrinsic permeability was determined by applying Klinkenberg's correction for gas slippage. Water sorptivity was measured by placing the sample in a tray containing water to a depth of about 3 mm above the bottom surface of the sample and then measuring the mass gain with time until saturation was achieved. The sorptivity coefficient ($g/m^2min^{0.5}$) was determined from the slope of the regression line of absorbed water per unit flow area against the square root of time ($R^2 > 0.99$) according to classical unsaturated flow theory.

## 3.0 RESULTS AND DISCUSSION

### 3.1 Failure mode

Two types of failure mode were observed during tensile splitting testing. Control samples with flat spacer-concrete interface failed through debonding as shown in Fig. 5a. However, samples with textured spacers failed via a combination of interface debonding and fracturing of the concrete as can be seen in Fig. 5b.

The failure mode and the maximum-recorded load for all samples are presented in Table 3. The results show that the failure load for samples with textured spacers increased by up to 53%, 98%, and 91.1% at 1, 7 and 28 days respectively, compared to those of the flat spacer. In other words, the presence of surface texture can drastically increase the failure load, especially for a longer curing age, when compared to the control sample without texturing.

a) Control (flat surface): Interface debonding.

b) Pyramid (PY) texture: Interface debonding and fracturing of the concrete

**Fig. 5.** Typical failure at spacer-concrete interface (left = spacer; right = concrete)

**Table 3.** Splitting tensile test results

| Texture type (abbreviation) | Failure mode (7d)* | Failure load (kN) | | |
|---|---|---|---|---|
| | | 1d | 7d | 28d |
| Control with flat surface (CO) | ID | 16.3 | 17.5 | 20.2 |
| Grooves-vertical (GV) | ID and FC | 19.9 | 23.8 | 28.3 |
| Grooves-horizontal (GH) | ID and FC | 19.7 | 22.9 | 23.9 |
| Half sphere (HS) | ID and FC | 21.1 | 31.5 | 36.4 |
| Pyramid (PY) | ID and FC | 24.9 | 34.6 | 38.6 |

*Note: ID = Interface debonding, FC = Fracturing of the concrete

### 3.2 Bond strength

Figure 6 shows the development of bond strength with curing age for all samples. The average length (L) and diameter (d) used in calculating all the bond strengths are 100 and 50 mm respectively. The results show that bond strength increases with curing age as expected. However, at all ages, the control sample with flat spacer consistently achieved lower bond strength compared to samples with textured spacers. The percentage difference ranges from 18 to 98%. Furthermore, samples with textured spacers showed a greater increase in bond strength with curing age compared to the control.

The highest bond strengths were achieved in samples with pyramid (PY) and half-sphere (HS) textured spacers. This is presumably because these textures have the largest profile depth and yield the largest contact surface area (see Table 2).

For samples with textured spacers, the concrete fills into the crevices of the spacer, forming a mechanical interlock that enhances bond strength. Therefore, failure occurs through a combination of debonding and fracturing. In contrast, such mechanical interlocking does not occur for flat spacers and so they bond weakly to the concrete and fail through debonding only. This will yield a weak interface that is prone to cracking, for example when the sample is subjected to tensile stresses induced by drying shrinkage or structural loading.

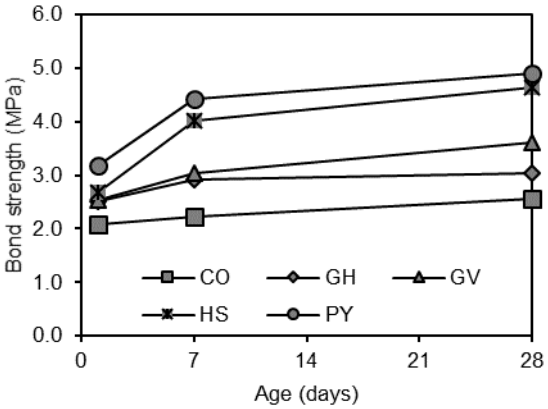


**Fig. 6.** Development of spacer-concrete bond strength with age for different surface textures

### 3.3 Relationship between surface parameters and interface bond strength

The interface bond between spacer and concrete is expected to be dependent on the surface geometry and the mechanical properties of both spacer and concrete. For example Fig. 7 shows the relationship between surface roughness ($A/A_o$) and bond strength. Here, surface roughness is defined as the ratio between the actual and projected surface areas.

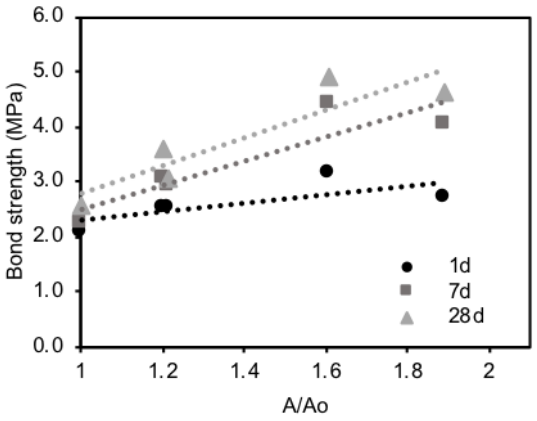


**Fig. 7.** Relationship between surface roughness ratio and interface bond strength

In another example, Fig. 8 presents the relationship between maximum profile depth and bond strength. These results show that bond strength increases with increasing surface roughness and profile depth. Interestingly, although the horizontal (GH) and vertical groove (GV) textures have the same surface roughness and profile depth, the latter produced slightly higher bond strength. This is probably due to the orientation of the GV-texture being perpendicular to the loading direction, leading to higher friction.

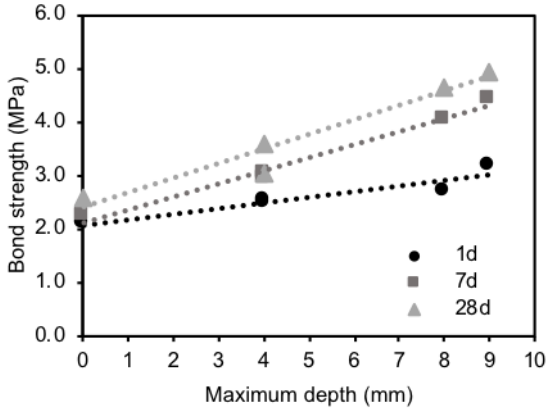


**Fig. 8.** Relationship between maximum profile depth and interface bond strength

To conclude, the surface texture of the spacer can enhance bond strength by promoting mechanical interlocking with the concrete. The overall strength of the spacer-concrete interface is dependent on the geometry, shape and orientation of the spacer surface texture.

### 3.4 Transport properties

The oxygen permeability, oxygen diffusivity, and water sorptivity of samples with different spacer-concrete interface after seven days of curing and conditioning at 50°C are presented in Fig. 9. The results suggest that the surface texture of the spacer does not have a consistent influence on mass transport. In some cases, textured spacers produce lower transport coefficients, while in others, the presence of textured spacers appears to increase transport properties relative to the control.

However, it is interesting to note that the sample with pyramid (PY) texture showed the lowest transport coefficients for all transport tests. This is consistent with the splitting tensile strength result showing the highest bond strength for this sample.

It is also interesting to note that the vertical grooves (GV) texture produced the highest transport properties, especially for permeability. This behaviour was probably caused by the direction of the grooves being parallel to the flow of gas/water.

Furthermore, surface defects in the form of air voids due to inadequate compaction were observed at the spacer-concrete interface (Fig. 10). Such defects are expected to influence transport properties in

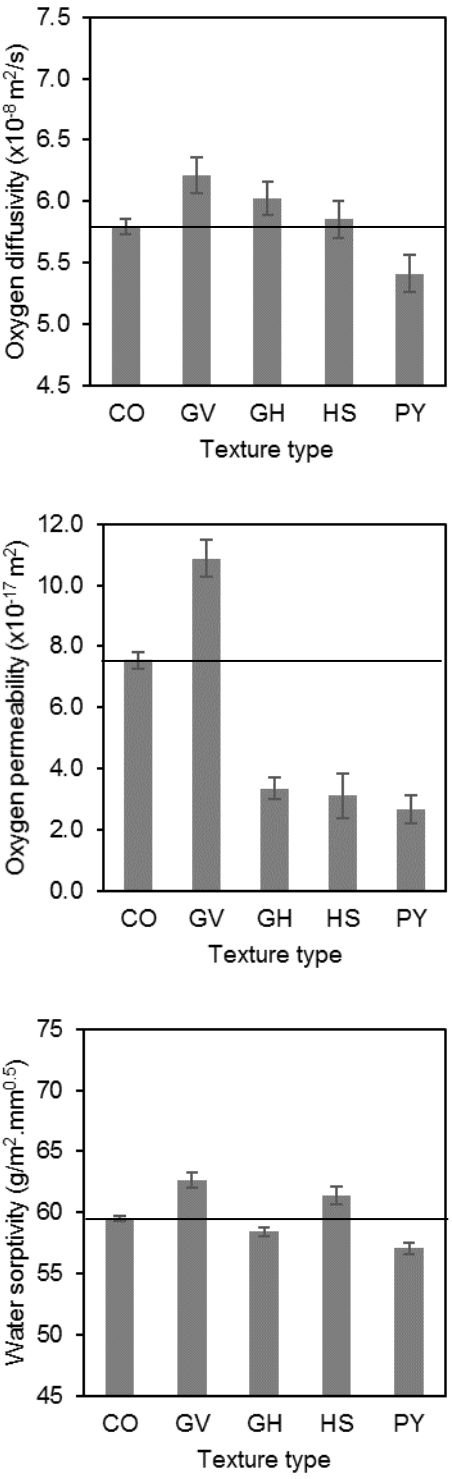


**Fig. 9.** Effect of surface texture on oxygen diffusivity, oxygen permeability, and water sorptivity

particular pressure-induced flow (Wong *et al.*, 2009, 2011). Permeability was most sensitive to changes in the spacer-concrete interface, and this is in line with previous results showing permeability being more sensitive to the presence of cracks compared to other transport properties (Wu *et al.*, 2014, 2015).

**Fig. 10.** Air voids at the spacer-concrete interface

## 4.0 CONCLUSIONS

This study showed that spacer surface texture has a clear effect on its interlocking with concrete and this can lead to a significant improvement in bond strength of the spacer-concrete interface. However, its effect on mass transport properties is less clear. Some surface textures increase the incidence of air voids at the interface, increasing transport properties and therefore outweighing their benefits. Further work is on-going to improve the understanding of this and to develop strategies to overcome the issue.

**Acknowledgement**

F. Muslim gratefully acknowledges the financial support for her PhD study provided by the Indonesian Endowment Fund for Education (LPDP). We thank Mr. Andrew Morris for his help with the laboratory work.

**References**

Alzyoud, S. *et al.*, 2016. Influence of reinforcement spacers on mass transport properties and durability of concrete structures, Cem. Concr. Res., 87:31-44.

BSI, 2001. Spacers and chairs for steel reinforcement and their specification. Product performance requirements. BS 7973 Part 1.

BSI, 2001. Spacers and chairs for steel reinforcement and their specification. Fixing and application of spacers and chairs and tying of reinforcement. BS 7973 Part 2.

BSI, 2009. Testing hardened concrete. Tensile splitting strength of test specimens. BS EN 12390 Part 6.

BSI, 2010. Assessment of surface texture. Guidance and general information. BS 1134.

Garbacz, A., Gorka, M., Courard, L., 2005. Effect of concrete surface treatment on adhesion in repair systems. Magazine of Concrete Research, 57(1):49-60.

Julio, E.N.B.S., Branco, F.A.B., Silva, V.D., 2004. Concrete-to-concrete bond strength. Influence of the roughness of the substrate surface. Construction and Building Materials, 18:675-681.

Pigeon, M. F. Saucier, 1992. Durability of repaired concrete structures. Advances in Concrete Technology, ed. by Malhotra VM: 741-773.

Wong, H.S. *et al.*, 2007. Mass transport properties of mature wasteform grouts. Advances in cement research, 19(1):35-46.

Wong, H.S. *et al.*, 2009. Influence of the interfacial transition zone and microcracking on the diffusivity, permeability and sorptivity of cement-based materials after drying. Magazine of concrete research, 61(8):571-589.

Wong, H.S. *et al.*, 2011. Effect of entrained air voids on the microstructure and mass transport properties of concrete, Cem. Concr. Res., 41:1067-1077.

Wu, Z. *et al.* (2014). Effect of confining pressure and microcracks on mass transport properties of concrete, Advances in Applied Ceramics, 113(8):485-495.

Wu, Z. *et al.* (2015), Influence of drying-induced microcracking and related size effects on mass transport properties of concrete, Cem. Concr. Res., 68:35-48.